SENSOR AND SIMULATION NOTES

Note 224

August 1976

Static Analysis of Conical Antenna Over a Ground Plane

Donald R. Wilton
University of Mississippi

ABSTRACT

A static integral equation for the charge distribution on a cone over a conducting ground plane is developed. Numerical results are presented for the charge distribution, capacitance, and effective height of cones both with and without a topcap.

CONTENTS

ILLUSTRATIONS

SECTION I

INTRODUCTION

One type of simulator used to simulate a vertically polarized electromagnetic pulse (EMP) produced by a nuclear detonation, is basically a conical antenna over a ground plane. Near the base of the bicone, the structure consists of a solid surface, constant flare angle bicone which gradually transitions into a wire biconical structure. While most of the current flow is radially directed along the wire portion of the bicone, circumferentially distributed wires are used to add to the capacitance per unit length as a wave travels along the bicone. The density of the circumferential wires and the wire bicone angle are then varied along the cone so as to make an equivalent bicone characteristic impedance at any point which roughly approximates that at the bicone input. A tapered resistive loading along the structure is used to damp out the high frequency currents along the antenna so as to minimize diffraction from the edge of the bicone. The present structure also has a flat topcap which is also loaded.

The circumferentially-directed wires are not orthogonal to the radially-directed wires and consequently most of the circumferential symmetry is destroyed. A moment method solution which would take into account all the wires and the solid surface feed region is thus unduly complicated for assessing the basic performance of the structure. In view of the intentional design of the structure, however, it seems reasonable to approximate the structure by a biconical surface whose flare angle is the same as that of the actual bicone feed region. In the following sections, then, a moment method solution procedure is used to obtain the static charge distributions, capacitances, and effective heights of bicones of various flare angles, both with and without topcaps. Derivation of the integral equation, formulation of the numerical solution procedure, and the numerical results follow in the succeeding sections.

SECTION II

FORMULATION OF THE INTEGRAL EQUATION

An integral equation for the charge on the bicone is obtained by requiring that the potential on the bicone, as produced by the charge, equal the driving potential between the cone surface and the ground plane. Referring to Figures 1-3, which define the appropriate geometrical quantities, one notes that the ground plane may be replaced by the bicone image on which a surface charge of the same distribution but of opposite sign exists. The resulting potential on the top biconical surface in terms of the charge, is then

$$\frac{1}{4\pi\varepsilon_0}\left[\int_0^{2\pi}\int_0^{L} \rho_c(r_c')\left(\frac{1}{R_{cc}^+}-\frac{1}{R_{cc}^-}\right) r_c' \sin\theta_0 dr_c' d\phi' + \int_0^{2\pi}\int_0^{L\sin\theta_0} \rho_t(r_t')\left(\frac{1}{R_{ct}^+}-\frac{1}{R_{ct}^-}\right) r_t' dr_t' d\phi'\right] = V_0. \tag{1a}$$

for observation points on the cone surface and

$$\frac{1}{4\pi\varepsilon_0}\left[\int_0^{2\pi}\int_0^{L} \rho_c(r_c')\left(\frac{1}{R_{tc}^+}-\frac{1}{R_{tc}^-}\right) r_c' \sin\theta_0 dr_c' d\phi' + \int_0^{2\pi}\int_0^{L\sin\theta_0} \rho_t(r_t')\left(\frac{1}{R_{tt}^+}-\frac{1}{R_{tt}^-}\right) r_t' dr_t' d\phi'\right] = V_0 \tag{1b}$$

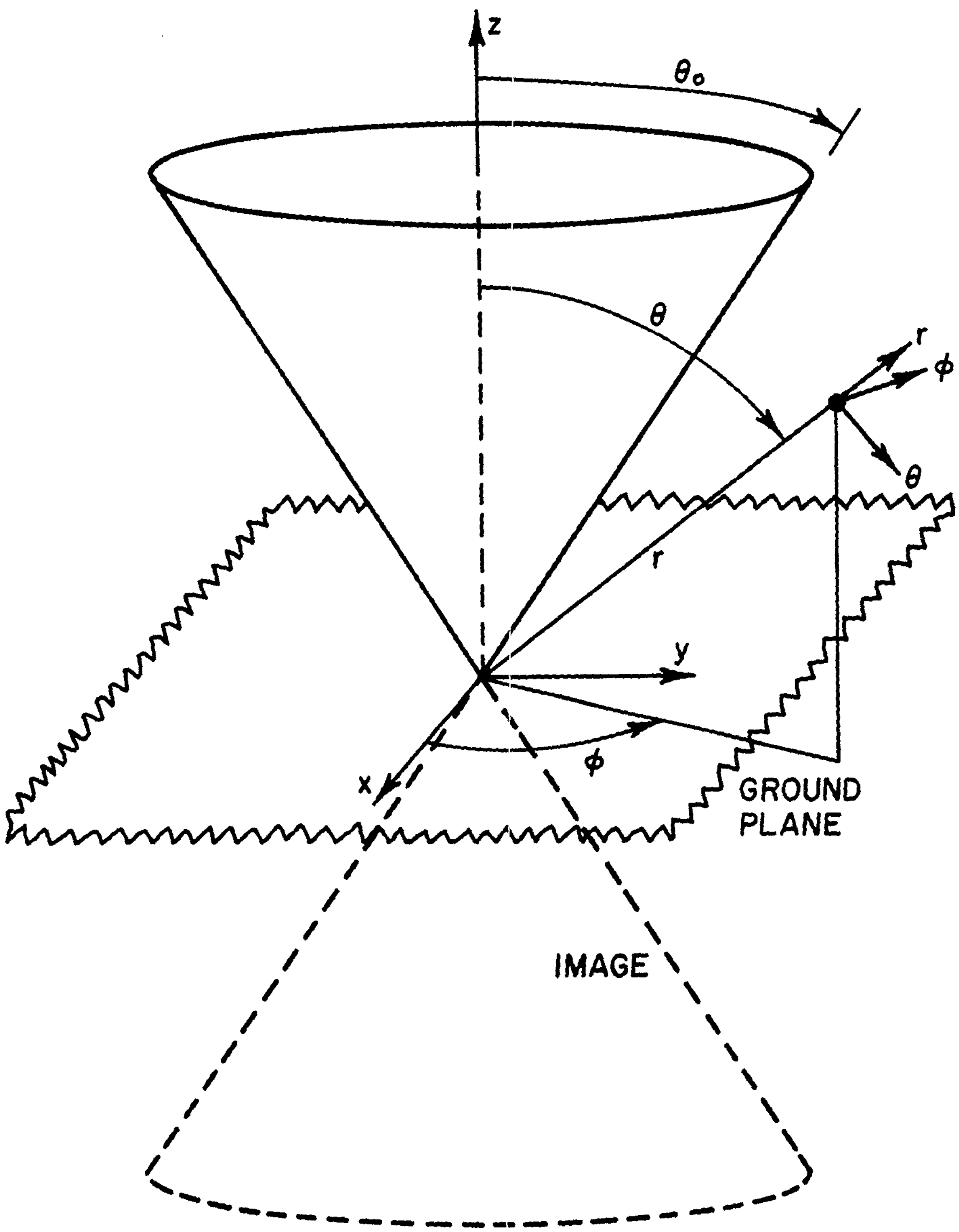

Figure 1. Geometry of cone over a ground plane.

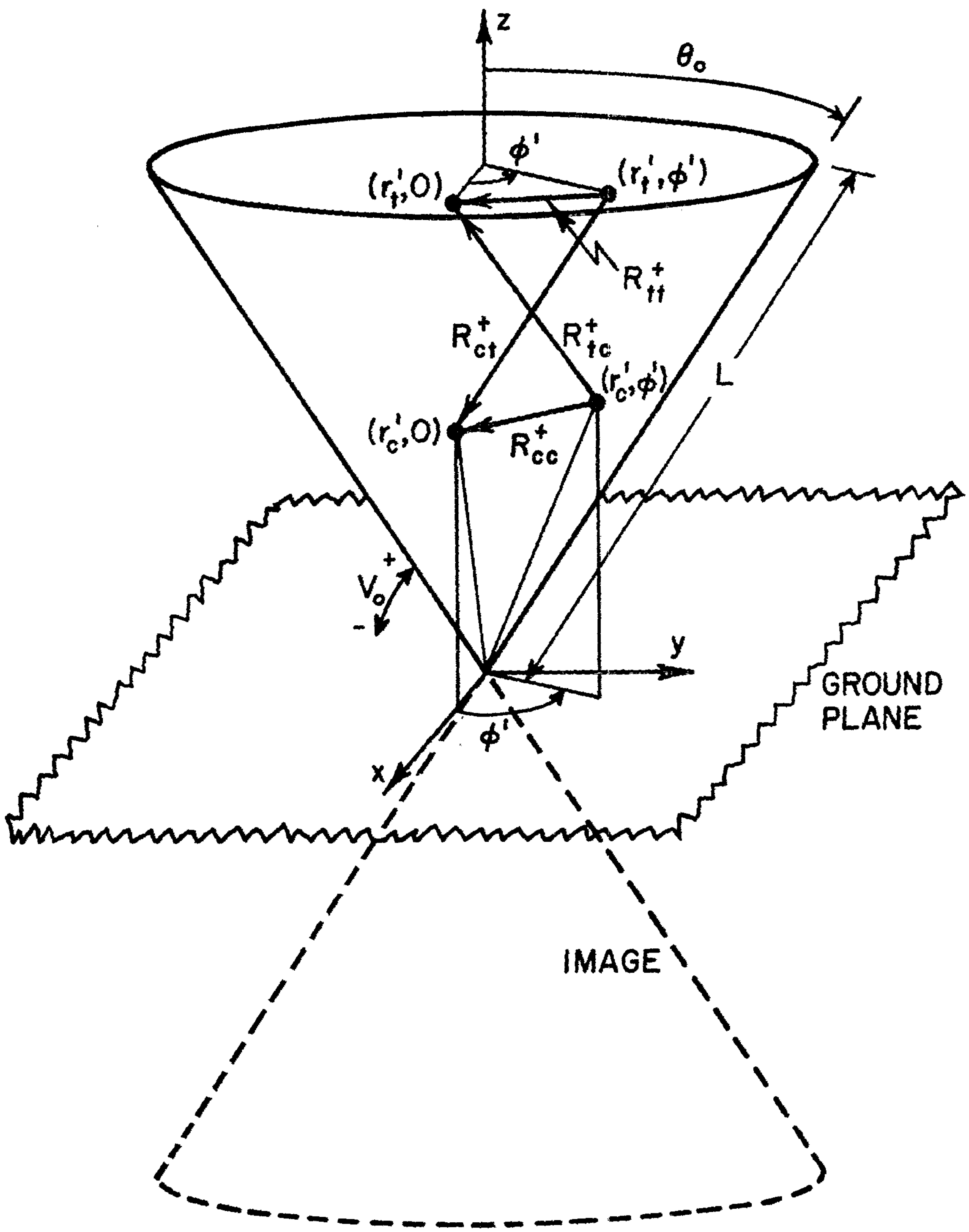

Figure 2. Field point, source point coordinates on cone above a ground plane.

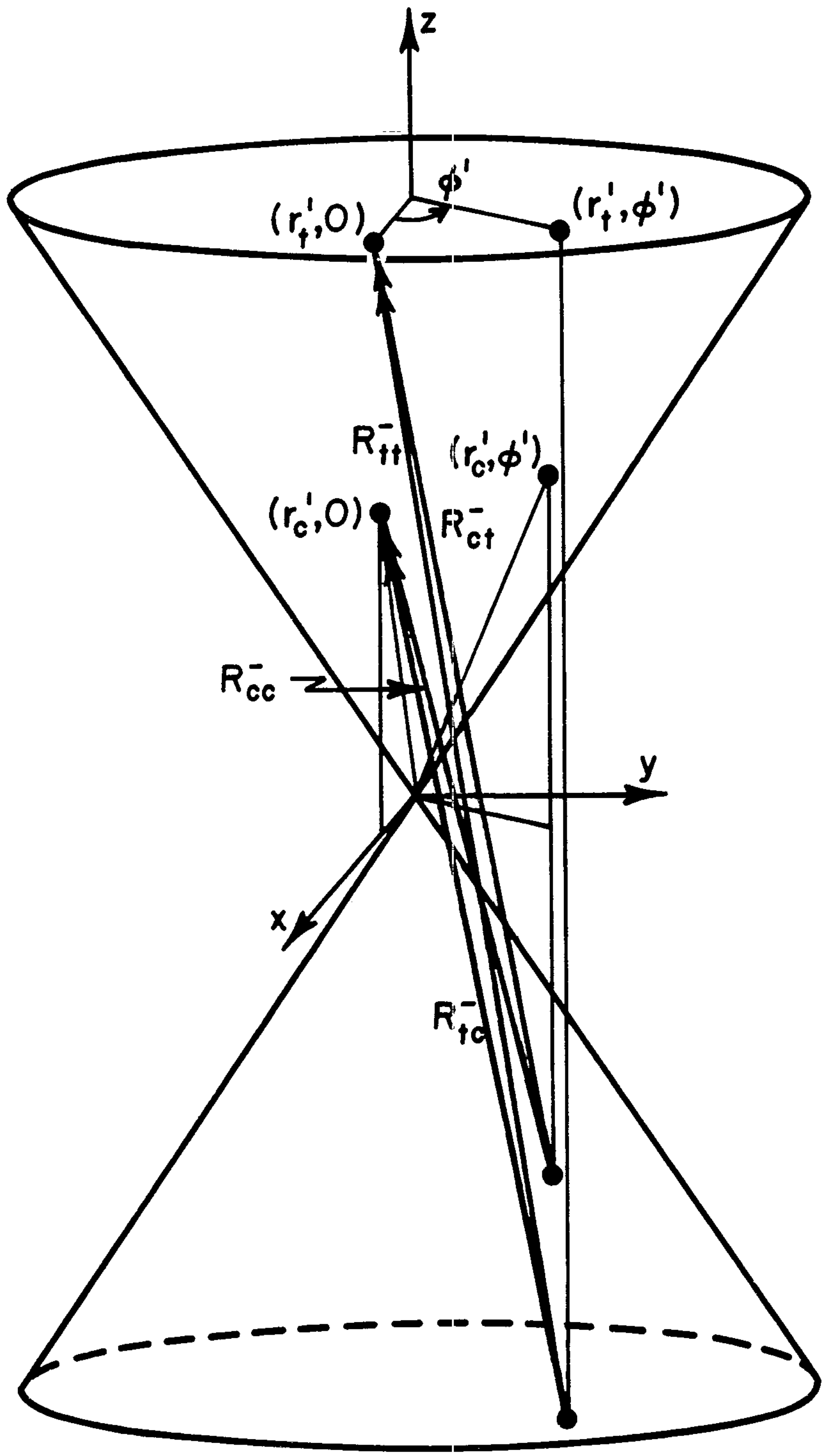

Figure 3. Field point, source point coordinates for the image cone.

for observation points on the topcap.

In (1), the subscripts c refer to quantities defined on the conical surface while subscripts t refer to the topcap. In double subscripted quantities, the first subscript refers to the surface on which the potential is observed while the second subscript denotes the origin of the source contributing to the potential. The plus and minus superscripts refer to source points on the cone and its image, respectively. If the cone has no topcap, only (1a) with ρ_t equal to zero is used. Since the fields are ϕ-symmetric, the observation points are taken along the x-z plane where $\phi=0$. The various distance quantities in terms of cone and topcap coordinates are all of the form

$$R^{\pm}_{rs} = \sqrt{A^{\pm}_{rs} - B_{rs} \cos \phi'}; \quad r,s = c,t \qquad (2)$$

where

$$A^{\pm}_{cc} = r_c^2 + r_c'^2 \mp 2 r_c r_c' \cos^2\theta_0$$

$$B_{cc} = 2 r_c r_c' \sin^2 \theta_0$$

$$A^{\pm}_{ct} = r_c^2 + r_t'^2 \mp 2r_c L \cos^2\theta_0 + L^2 \cos^2\theta_0$$

$$B_{ct} = 2r_c r_t' \sin \theta_0$$

$$A^{\pm}_{tc} = r_t^2 + r_c'^2 \mp 2r_c' L \cos^2\theta_0 + L^2 \cos^2\theta_0$$

$$B_{tc} = 2r_t r_c' \sin \theta_0$$

$$A_{tt}^{\pm} = r_t^2 + r_t'^2 + L^2 \cos^2\theta_0(1 \mp 1)^2$$

$$B_{tt} = 2r_t r_t' \tag{3}$$

The linear charge densities

$$q_c(r_c) = 2\pi r_c \sin\theta_0 \rho_c(r_c) \tag{4a}$$

$$q_t(r_t) = 2\pi r_t \rho_t(r_t) \tag{4b}$$

may alternatively be used. Since the charge density is ϕ-independent, the ϕ integrations may also be performed in (1). These involve integrals of the form

$$\int_0^{2\pi} \frac{d\phi'}{R} = \int_0^{2\pi} \frac{d\phi'}{\sqrt{A-B\cos\phi'}}$$

$$= 2\int_0^{\pi} \frac{d\phi'}{\sqrt{A-B\cos\phi'}}$$

$$= 2\int_0^{\pi} \frac{d\phi'}{\sqrt{A+B\cos\phi'}}$$

$$= 2\int_0^{\pi} \frac{d\phi'}{\sqrt{A+B-2B\sin^2\phi'/2}}$$

$$= 4\int_0^{\pi/2} \frac{d\xi}{\sqrt{A+B - 2B\sin^2\xi}}$$

$$= \frac{4}{(A+B)^{\frac{1}{2}}} K\left(\frac{2B}{A+B}\right) \tag{5}$$

where

$$K(m) = \int_0^{\pi/2} \frac{d\xi}{\sqrt{1 - m\sin^2\xi}} \tag{6}$$

is the complete elliptic integral of the first kind. Hence, using (5) and (4), (1) can be written as

$$\frac{1}{2\pi^2\varepsilon_0}\left\{\int_0^L q_c(r_c')\left[\frac{K\left(\frac{2B_{cc}}{A_{cc}^+ + B_{cc}}\right)}{(A_{cc}^+ + B_{cc})^{\frac{1}{2}}} - \frac{K\left(\frac{2B_{cc}}{A_{cc}^- + B_{cc}}\right)}{(A_{cc}^- + B_{cc})^{\frac{1}{2}}}\right]dr_c'\right.$$

$$\left. + \int_0^{L\sin\theta_0} q_t(r_t')\left[\frac{K\left(\frac{2B_{ct}}{A_{ct}^+ + B_{ct}}\right)}{(A_{ct}^+ + B_{ct})^{\frac{1}{2}}} - \frac{K\left(\frac{2B_{ct}}{A_{ct}^- + B_{ct}}\right)}{(A_{ct}^- + B_{ct})^{\frac{1}{2}}}\right]dr_t'\right\} = V_0 \tag{7a}$$

$$\frac{1}{2\pi^2\varepsilon_0}\left\{\int_0^L q_c(r_c')\left[\frac{K\left(\frac{2B_{tc}}{A_{tc}^+ + B_{tc}}\right)}{(A_{tc}^+ + B_{tc})^{\frac{1}{2}}} - \frac{K\left(\frac{2B_{tc}}{A_{tc}^- + B_{tc}}\right)}{(A_{tc}^- + B_{tc})^{\frac{1}{2}}}\right]dr_c'\right.$$

$$\left. + \int_0^{L\sin\theta_0} q_t(r_t')\left[\frac{K\left(\frac{2B_{tt}}{A_{tt}^+ + B_{tt}}\right)}{(A_{tt}^+ + B_{tt})^{\frac{1}{2}}} - \frac{K\left(\frac{2B_{tt}}{A_{tt}^- + B_{tt}}\right)}{(A_{tt}^- + B_{tt})^{\frac{1}{2}}}\right]dr_t'\right\} = V_0 \tag{7b}$$

Once the linear charge densities q_c and q_t are known the total bicone-to-ground capacitance C is found as

$$C = \frac{Q_{tot}}{V_0} \tag{8}$$

and the effective height is given by

$$h_{eff} = \frac{\cos\theta_0 \left[\int_0^L q_c(r_c') r_c' dr_c' + L \int_0^{L \sin\theta_0} q_t(r_t') dr_t' \right]}{Q_{tot}} \tag{9}$$

where the total charge on the bicone is

$$Q_{tot} = \int_0^L q_c(r_c') dr_c' + \int_0^{L \sin\theta_0} q_t(r_t') dr_t' \tag{10}$$

SECTION III

NUMERICAL SOLUTION PROCEDURE

The method of moments [1] is used to obtain a numerical solution to the integral equation (7). Since at the bicone feed, the linear charge density approaches that of the infinite static bicone, whereas the surface charge density is infinite there, it is appropriate to expand the linear charge in constant pulse functions on the conical surface. On the topcap, however, the surface charge density approaches a constant at the center of the cap while the linear charge density varies linearly there. Hence, on the topcap, the unknown is taken to be the surface charge density, which is expanded in pulse functions. Figure 4 shows the pulse expansion scheme used. Subdomains of widths

$$\Delta r_c = \frac{L}{N_c} \tag{11a}$$

and

$$\Delta r_t = \frac{L \sin \theta_0}{N_t} \tag{11b}$$

are used on the cone and topcap surfaces, respectively. The subdomains are centered at the points

$$r_{cm} = (m - \tfrac{1}{2})\Delta r_c, \quad m=1,2,\ldots, N_c \tag{12a}$$

on the cone surface and at

$$r_{tn} = (n - \tfrac{1}{2})\Delta r_t, \quad n=1,2,\ldots, N_t \tag{12b}$$

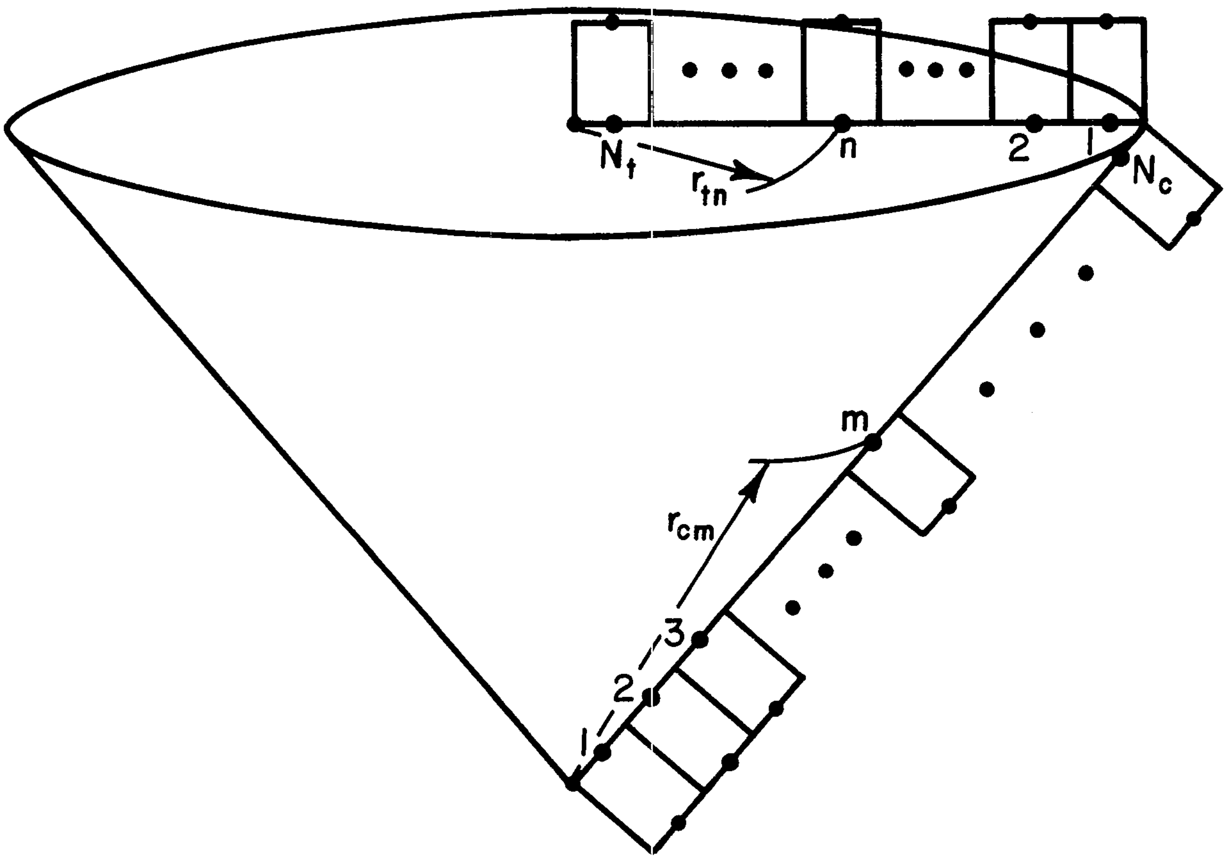

Figure 4. Pulse expansion scheme for the charge on the upper cone.

on the topcap surface.

Endpoints of the subdomains are at

$$r_{cm\pm} = r_{cm} \pm \Delta r_{c/2} \tag{13a}$$

$$r_{tn\pm} = r_{tn} \pm \Delta r_{t/2} \tag{13b}$$

If we define a unit pulse function

$$p(x) = \begin{cases} 1, & |x| \leq \frac{1}{2} \\ 0, & |x| > \frac{1}{2} \end{cases} \tag{14}$$

then the charge expansions may be written as

$$q_c \simeq \sum_{m=1}^{N_c} Q_{cm}\ p\left(\frac{r_c - r_{cm}}{\Delta r_c}\right) \tag{15a}$$

$$\rho_t \simeq \sum_{n=1}^{N_t} Q_{tn}\ p\left(\frac{r_t - r_{tn}}{\Delta r_t}\right) \tag{15b}$$

where the quantities Q_{cm} and Q_{tn} are the linear and surface charge densities in the center of the mth and nth subdomains on the cone and topcap, respectively. Substituting (15) into (7), using (4b), and enforcing the equality on both sides of (7) at the centers of the subdomains results in the matrix equation

$$\left[\begin{array}{c|c} C_{cc} & C_{ct} \\ \hline C_{tc} & C_{tt} \end{array}\right] \left[\begin{array}{c} Q_c \\ \hline Q_t \end{array}\right] = \left[\begin{array}{c} V_c \\ \hline V_t \end{array}\right] \tag{16}$$

for the coefficients Q_{cm} and Q_{tn}, where the column vectors of unknowns are

$$Q_c = \begin{bmatrix} Q_{c2} \\ \vdots \\ Q_{cm} \\ \vdots \\ Q_{cN_c} \end{bmatrix} \quad Q_t = \begin{bmatrix} Q_{t1} \\ \vdots \\ Q_{tm} \\ \vdots \\ Q_{tN_t} \end{bmatrix}, \tag{17}$$

and the driving vectors are

$$V_c = \begin{bmatrix} V_0 \\ \vdots \\ V_0 \end{bmatrix}, \quad V_t = \begin{bmatrix} V_0 \\ \vdots \\ V_0 \end{bmatrix} \tag{18}$$

The elements of the "capacitance matrix" are

$$(C_{cc})_{pm} = \frac{1}{2\pi^2\varepsilon_0} \psi_{cc}(r_{cp}, r_{cm})$$

$$(C_{ct})_{pn} = \frac{1}{\pi\varepsilon_0} \psi_{ct}(r_{cp}, r_{tn})$$

$$(C_{tc})_{qm} = \frac{1}{2\pi^2\varepsilon_0} \psi_{tc}(r_{tq}, r_{cm}) \tag{19}$$

$$(C_{tt})_{qn} = \frac{1}{\pi\varepsilon_0} \psi_{tt}(r_{tq}, r_{tn})$$

$$p, m = 1, 2, \ldots, N_c$$

$$q, n = 1, 2, \ldots, N_t$$

where

$$\psi_{cc}(r_{cp}, r_{cm}) = \int_{r_{cm}^-}^{r_{cm}^+} \left[\frac{K\left(\dfrac{2B_{cc}}{A_{cc}^+ + B_{cc}}\right)}{(A_{cc}^+ + B_{cc})^{\frac{1}{2}}} - \frac{K\left(\dfrac{2B_{cc}}{A_{cc}^- + B_{cc}}\right)}{(A_{cc}^- + B_{cc})^{\frac{1}{2}}} \right] dr_c' \Bigg|_{r_c = r_{cp}}$$

$$\psi_{ct}(r_{cp},r_{tn}) = \int_{r_{tn}^-}^{r_{tn}^+} \left[\frac{K\left(\dfrac{2B_{ct}}{A_{ct}^+ + B_{ct}}\right)}{(A_{ct}^+ + B_{ct})^{\frac{1}{2}}} - \frac{K\left(\dfrac{2B_{ct}}{A_{ct}^- + B_{ct}}\right)}{(A_{ct}^- + B_{ct})^{\frac{1}{2}}} \right] r_t' dr_t' \Bigg|_{r_c = r_{cp}}$$

$$\psi_{tc}(r_{tq},r_{cm}) = \int_{r_{cm}^-}^{r_{cm}^+} \left[\frac{K\left(\dfrac{2B_{tc}}{A_{tc}^+ + B_{tc}}\right)}{(A_{tc}^+ + B_{tc})^{\frac{1}{2}}} - \frac{K\left(\dfrac{2B_{tc}}{A_{tc}^- + B_{tc}}\right)}{(A_{tc}^- + B_{tc})^{\frac{1}{2}}} \right] dr_c' \Bigg|_{r_t = r_{tq}}$$

$$\psi_{tt}(r_{tq},r_{tn}) = \int_{r_{tn}^-}^{r_{tn}^+} \left[\frac{K\left(\dfrac{2B_{tt}}{A_{tt}^+ + B_{tt}}\right)}{(A_{tt}^+ + B_{tt})^{\frac{1}{2}}} - \frac{K\left(\dfrac{2B_{tt}}{A_{tt}^- + B_{tc}}\right)}{(A_{tt}^- + B_{tt})^{\frac{1}{2}}} \right] r_t' dr_t' \Bigg|_{r_t = r_{tq}} \tag{20}$$

When p=m and when q=n, the integrands of ψ_{cc} and ψ_{tt}, respectively, are logarithmically singular:

$$\frac{K\left(\dfrac{2B_{cc}}{A_{cc}^+ + B_{cc}}\right)}{(A_{cc}^+ + B_{cc})^{\frac{1}{2}}} \xrightarrow[r_c' \to r_{cp}]{} - \frac{\ell n|r_c' - r_{cp}|}{2r_{cp} \sin\theta_0}$$

$$\frac{K\left(\dfrac{2B_{tt}}{A_{tt}^+ + B_{tt}}\right)}{(A_{tt}^+ + B_{tt})^{\frac{1}{2}}} \xrightarrow[r_t' \to r_{tq}]{} - \frac{\ell n|r_t' - r_{tq}|}{2r_{tq}}$$

These terms are thus handled numerically by subtracting out the singularity from the integrand and adding its analytically evaluated integral as follows:

$$\psi_{cc}(r_{cp},r_{cp}) = \int_{r_{cp^-}}^{r_{cp^+}} \left[\frac{K\left(\dfrac{2B_{cc}}{A_{cc}^{+} + B_{cc}}\right)}{(A_{cc}^{+} + B_{cc})^{\frac{1}{2}}} + \frac{\ln|r_c' - r_{cp}|}{2r_{cp}\sin\theta_0} - \frac{K\left(\dfrac{2B_{cc}}{A_{cc}^{-} + B_{cc}}\right)}{(A_{cc}^{-} + B_{cc})^{\frac{1}{2}}} \right] dr_c' \Bigg|_{r_c' = r_{cp}}$$

$$+ \frac{\Delta r_c}{2r_{cp}\sin\theta_0}\left(1 - \ln\left(\frac{\Delta r_c}{2}\right)\right) \qquad (21a)$$

$$\psi_{tt}(r_{tq},r_{tq}) = \int_{r_{tq^-}}^{r_{tq^+}} \left[\frac{K\left(\dfrac{2B_{tt}}{A_{tt}^{+} + B_{tt}}\right)}{(A_{tt}^{+} + B_{tt})^{\frac{1}{2}}} + \frac{\ln|r_t' - r_{tq}|}{2r_{tq}} - \frac{K\left(\dfrac{2B_{tt}}{A_{tt}^{-} + B_{tt}}\right)}{(A_{tt}^{-} + B_{tt})^{\frac{1}{2}}} \right] dr_t' \Bigg|_{r_t' = r_{tq}}$$

$$+ \frac{\Delta r_t}{2r_{tq}}\left(1 - \ln\left(\frac{\Delta r_t}{2}\right)\right) \qquad (21b)$$

The resulting integrands in (21) are non-singular and may be numerically integrated using standard methods. Solution of the $(p+q)\times(p+q)$ matrix equation (16) yields the charge coefficients Q_{cm} and Q_{tn}. Recall that the former is a linear charge density quantity while the latter is a surface charge density. Equations (4) give the formulas for conversion between surface and linear charge density quantities. From (9) and (10) the capacitance to ground and effective height are calculated as

$$C = \frac{Q_{tot}}{V_0}, \qquad (21)$$

$$h_{eff} = \frac{\cos\theta_0 \left[\Delta r_c \sum_{m=1}^{N_c} Q_{cm} r_{cm} + 2\pi L \Delta r_t \sum_{n=1}^{N_t} Q_{tn} r_{tn} \right]}{Q_{tot}} \qquad (22)$$

where

$$Q_{tot} = \Delta r_c \sum_{m=1}^{N_c} Q_{cm} + 2\pi\Delta r_t \sum_{n=1}^{N_t} Q_{tn} r_{tn} \qquad (23)$$

SECTION III

NUMERICAL RESULTS

In this section, numerical results are presented for the linear charge distribution, capacitance, and effective height of a cone over a ground plane as the cone angle, θ_0, is varied. Results are given for configurations both with and without a topcap. For convenience in simulator design, the data is presented assuming the permittivity of free space rather than normalizing the data to a medium independent form. However, for other applications, the data can easily be scaled to apply to isotropic, homogeneous media with permittivities different from that of free space.

In Figures 5, 6, and 7, the linear charge density is plotted for various cone angles ranging between $\theta_0 = 2.5°$ and $\theta_0 = 85°$. Note that as the cone length L tends to infinity, the linear charge density at any point on the cone should tend to that of an infinite cone over a ground plane,

$$q \xrightarrow[L\to\infty]{} \frac{2\pi\varepsilon_0 V_0}{\ln \cot(\frac{\theta_0}{2})} \tag{24}$$

where V_0 is the voltage between the cone and ground plane or half the voltage across the terminals of a bicone structure. Since, for the static problem, only relative dimensions are important, $L\to\infty$ is equivalent to $r_c \to 0$, since from either point

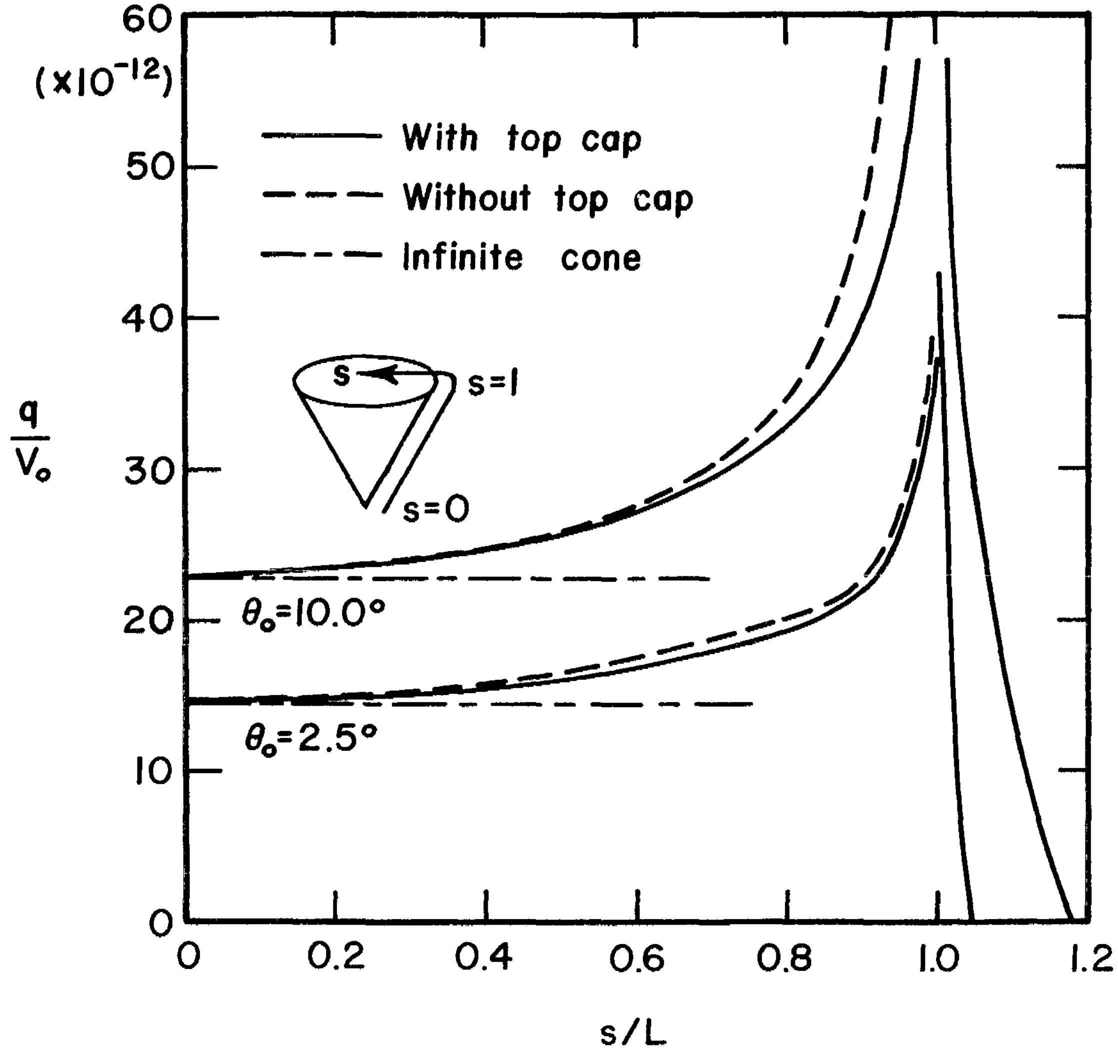

Figure 5. Linear charge density on a charged cone, θ_0=2.5°, 10°.

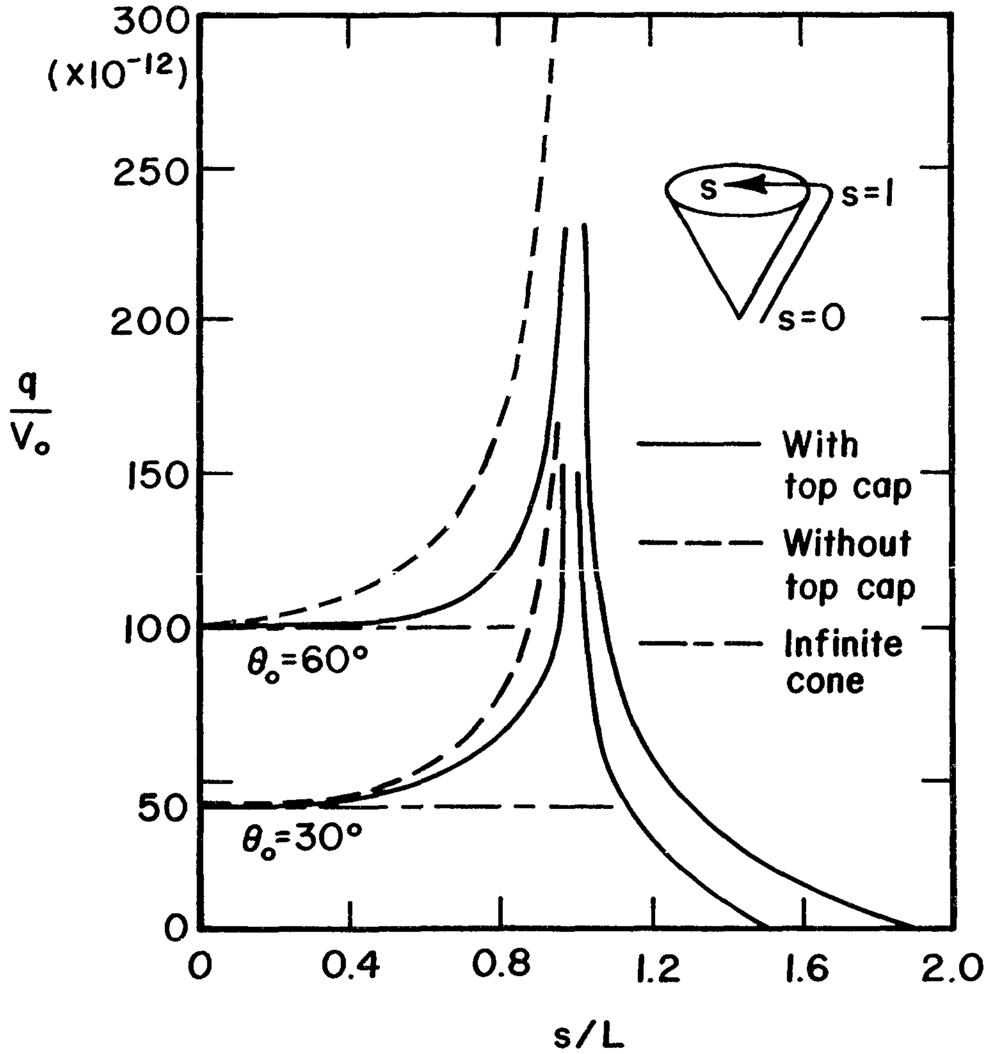

Figure 6. Linear charge density on a charged cone, θ_0=30°, 60°.

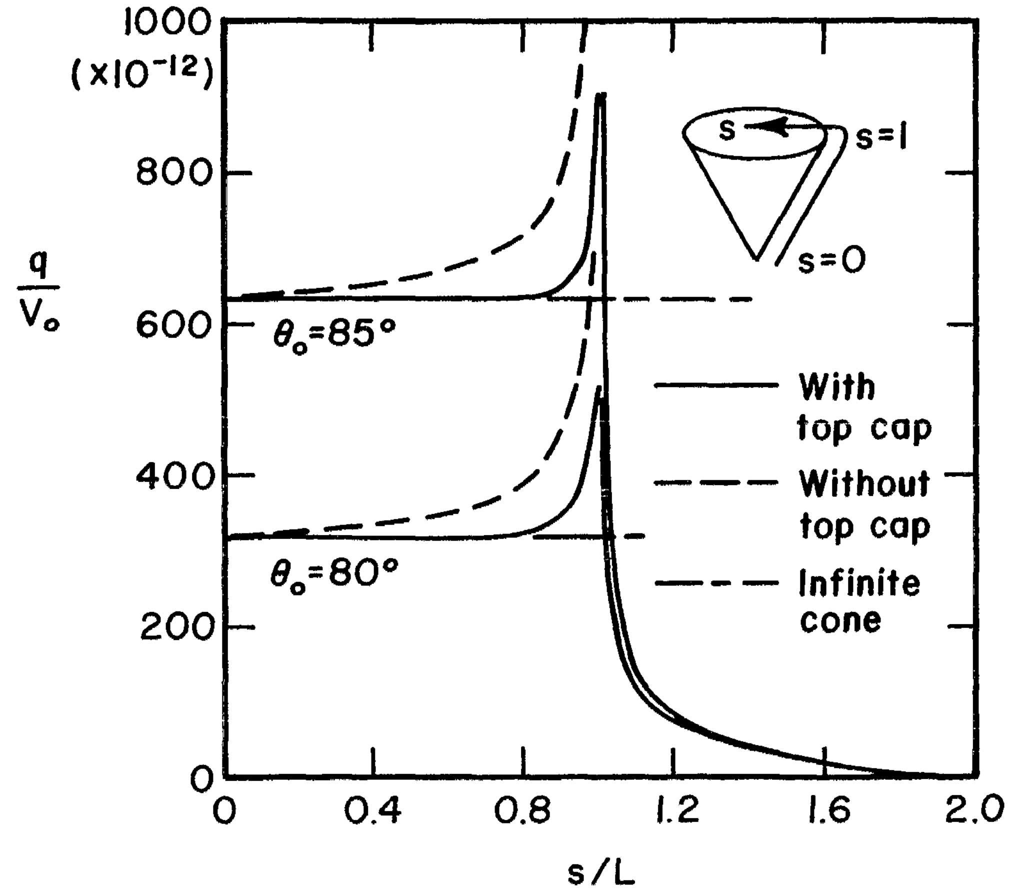

Figure 7. Linear charge density on a charged cone, θ_0=80°,85°.

of view, $r_c/L \to 0$. Thus the numerically computed results should approach (24) as $r_c \to 0$ and this limit, also shown in Figures 5, 6 and 7, provided a convenient check on the numerical results. Note that for narrow cone angles (Figure 5), there is very little charge on the topcap, as one would expect. For large cone angles (Figure 7), note that the charge on the topcap approximates the increase in the charge on the cone without a topcap. The total charge in the latter case includes, of course, the charge on the top surface of the cone. For moderate cone angles (Figure 6), a substantial portion of the total charge resides on the topcap. With no topcap, however, the edge condition [2] requires a more singular charge at the edge of the cone. Furthermore, the computed charge in this case is the sum of the charge densities on both sides of the cone surface. The net result is that the total charge, with or without the topcap, is roughly the same for all cone angles. This is strikingly evident in Table 1 in which is tabulated the capacitance of a cone with and without a topcap for various cone angles normalized both to the slant height and the vertical height of the cone. From the tables, it appears that the addition of a topcap increases the total capacitance only by about 3% for moderate cone angles. The computed capacitances agree fairly well with the rough estimates used in [3].

Table 1. Computed Capacitance of a Cone over a Conducting Ground Plane

θ_0	With Topcap C/L (μμf/m)	With Topcap C/L cos θ_0 (μμf/m)	Without Topcap C/L (μμf/m)	Without Topcap C/L cos θ_0 (μμf/m)
2.5°	18.68	18.69	18.54	18.55
5.0°	24.32	24.41	24.06	24.15
10.0°	34.02	34.54	33.42	33.94
15.0°	43.22	44.74	42.24	43.73
20.0°	52.51	55.88	51.10	54.38
30.0°	72.16	83.32	69.84	80.64
40.0°	94.40	123.2	91.23	119.1
50.0°	121.5	189.0	117.7	183.1
60.0°	158.8	317.6	154.7	309.4
70.0°	222.5	650.6	218.6	639.1
80.0°	393.9	2,268.	391.0	2,252.
85.0°	721.2	8,275.	719.2	8,252.
87.5°	1,360.	31,180.	1,358.	31,130.

In Figures 8-11, the capacitance of the cone is plotted as a function of the cone angle, with and without a topcap. In Figures 8 and 10, the capacitances are normalized to the slant height, whereas in Figures 9 and 11, the capacitances are normalized to the vertical height of the structure. Also shown are the corresponding capacitances, C_∞, that would be computed assuming the charge distribution to be that of an infinite bicone, Eq. (24). Using (24), C_∞ is easily found to be

$$C_\infty = \frac{2\pi\varepsilon_0 L}{\ell n \cot \frac{\theta_0}{2}} \tag{25}$$

The excess or "fringing" capacitance is then just $C - C_\infty$. As a matter of interest and as a check on the reasonableness of the computed capacitances, the percentage of fringing capacitance is plotted in Figures 12 and 13 as a function of θ_0. As would be expected, the percentage of the capacitance attributable to fringing is smallest for cone angles near 0° and 90°. Near $\theta_0 = 40°$, the fringing capacitance adds 70% of C_∞ to the total capacitance.

Table 2 lists the effective height of a cone structure with and without a topcap. Note that since the linear charge density on an infinite cone is constant, Eq. (24), the computed effective height neglecting fringing would be $L\cos\theta_0/2$. Since the fringing fields increase the charge density near the cone edge, this figure is a lower bound on the effective height but is approached as θ_0 tends to 0° and 90°.

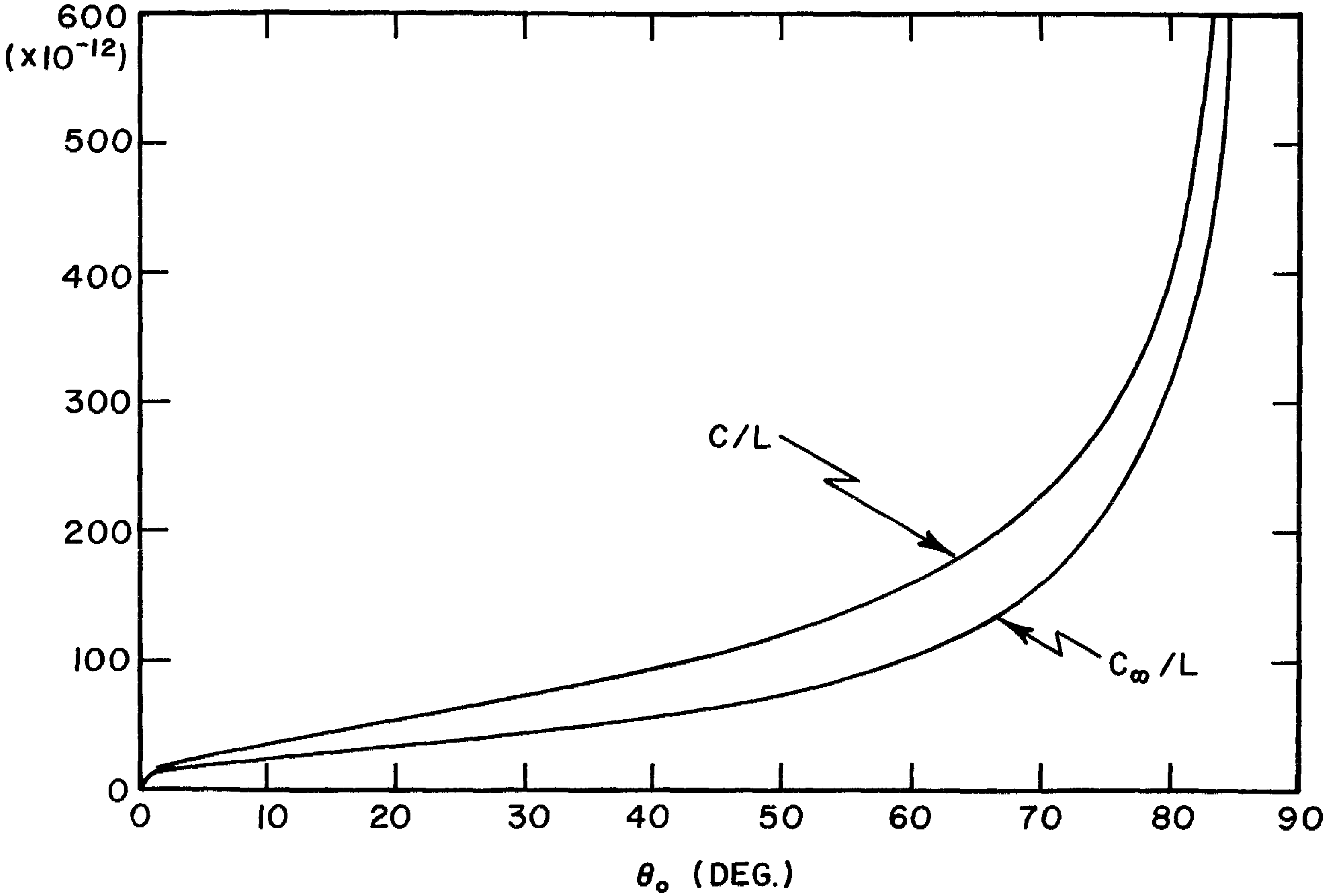

Figure 8. Capacitance normalized to the slant height of a cone with a topcap.

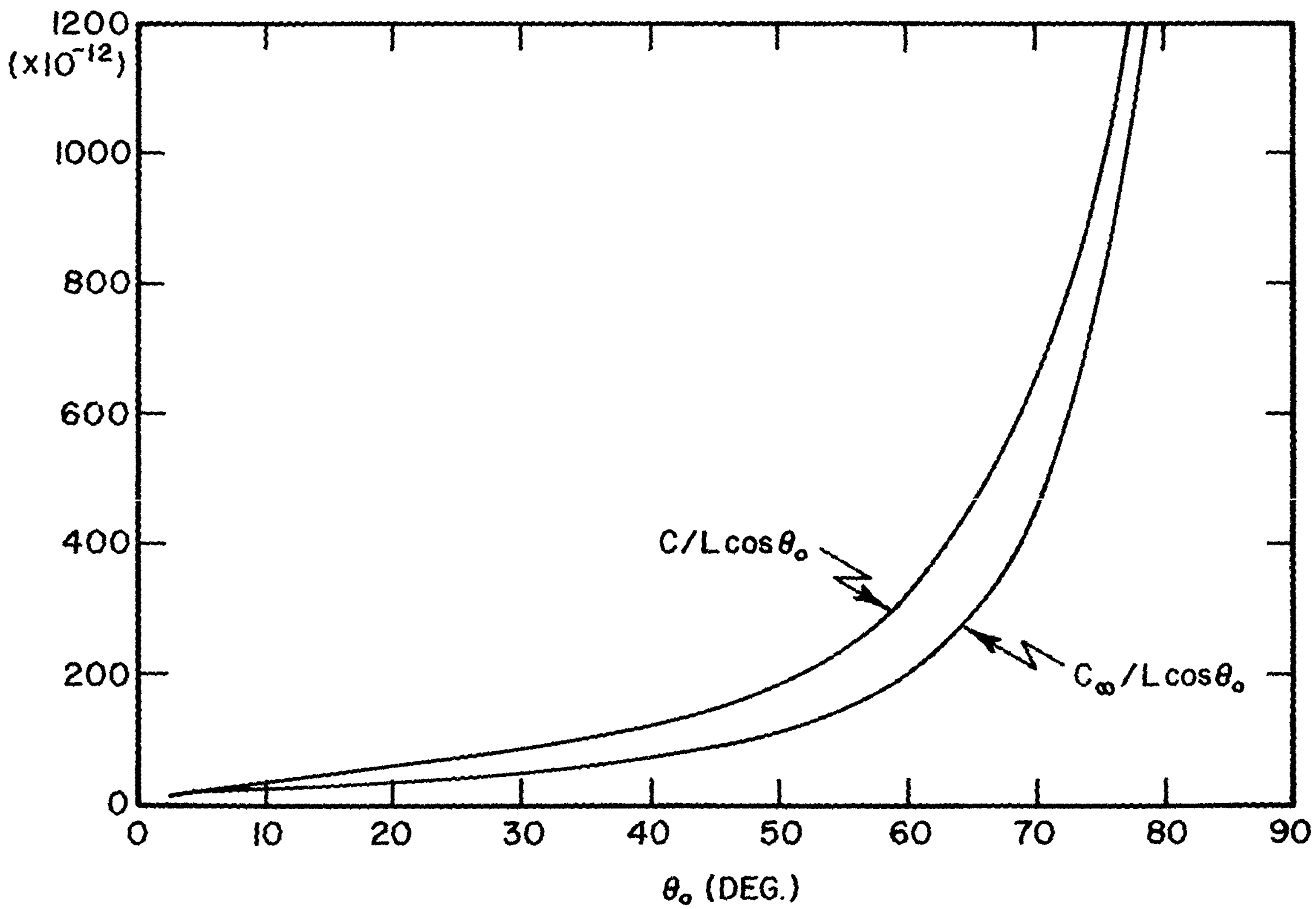

Figure 9. Capacitance normalized to the vertical height of a cone with a topcap.

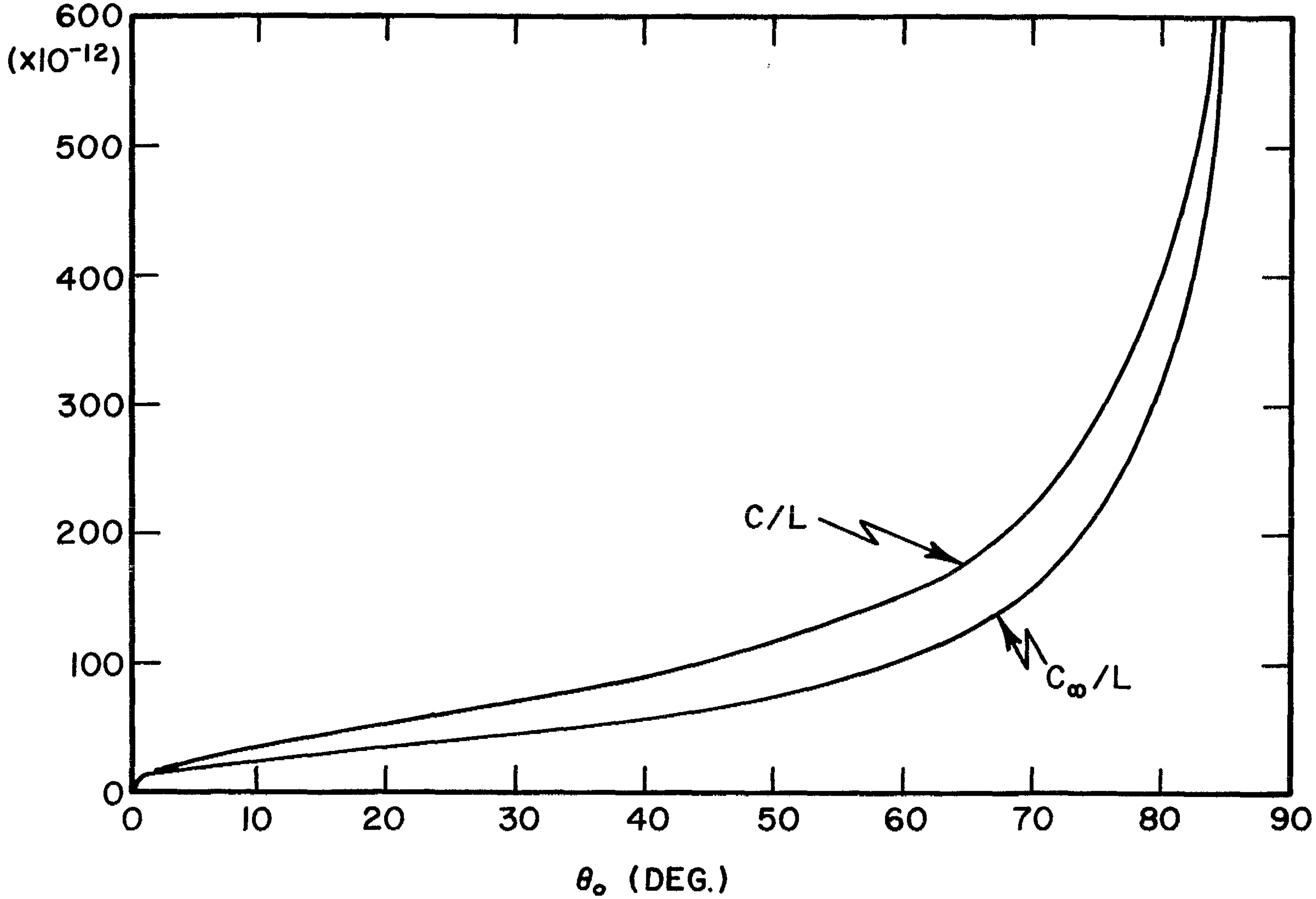

Figure 10. Capacitance normalized to the slant height of a cone without a topcap.

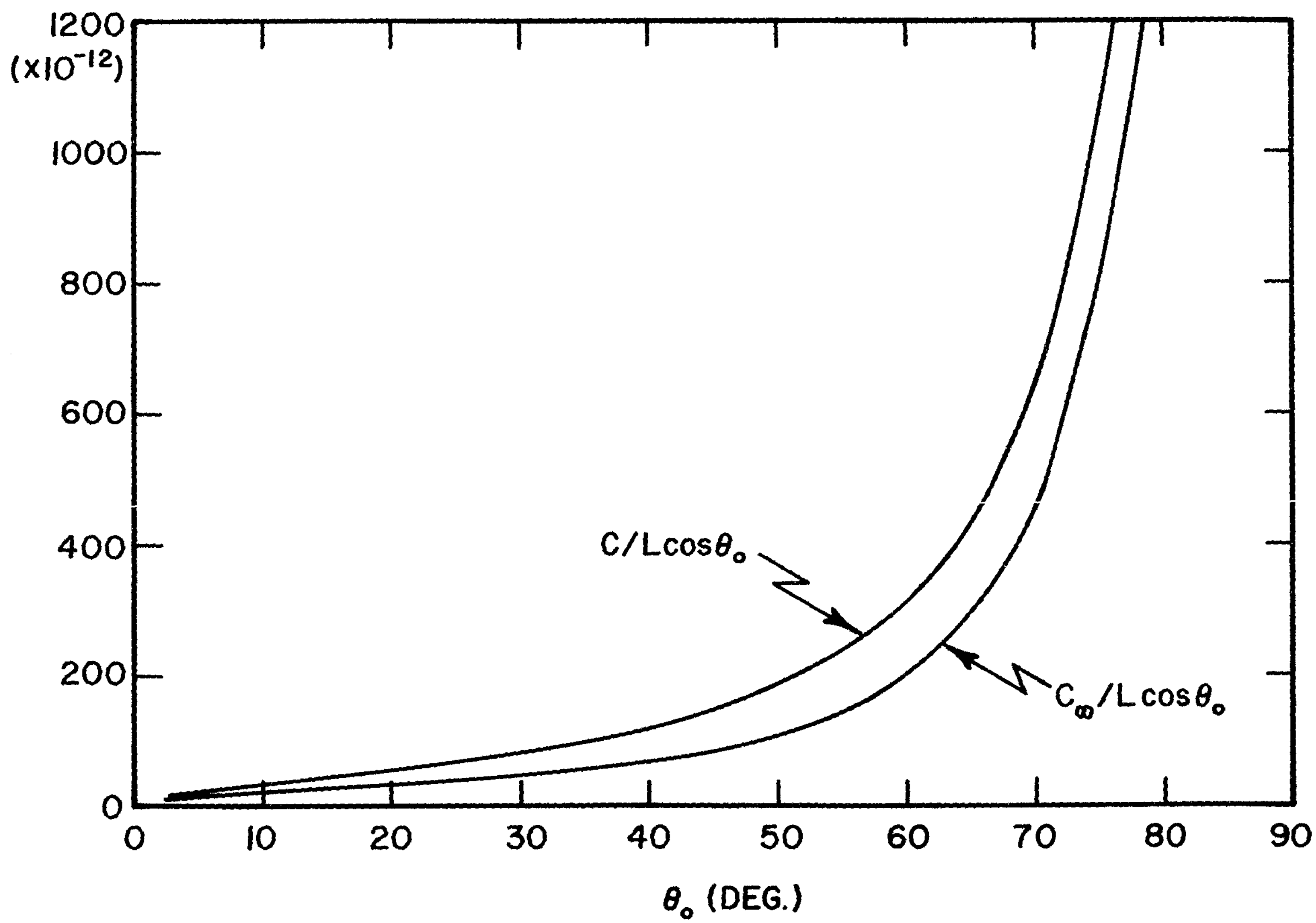

Figure 11. Capacitance normalized to the vertical height of a cone without a topcap.

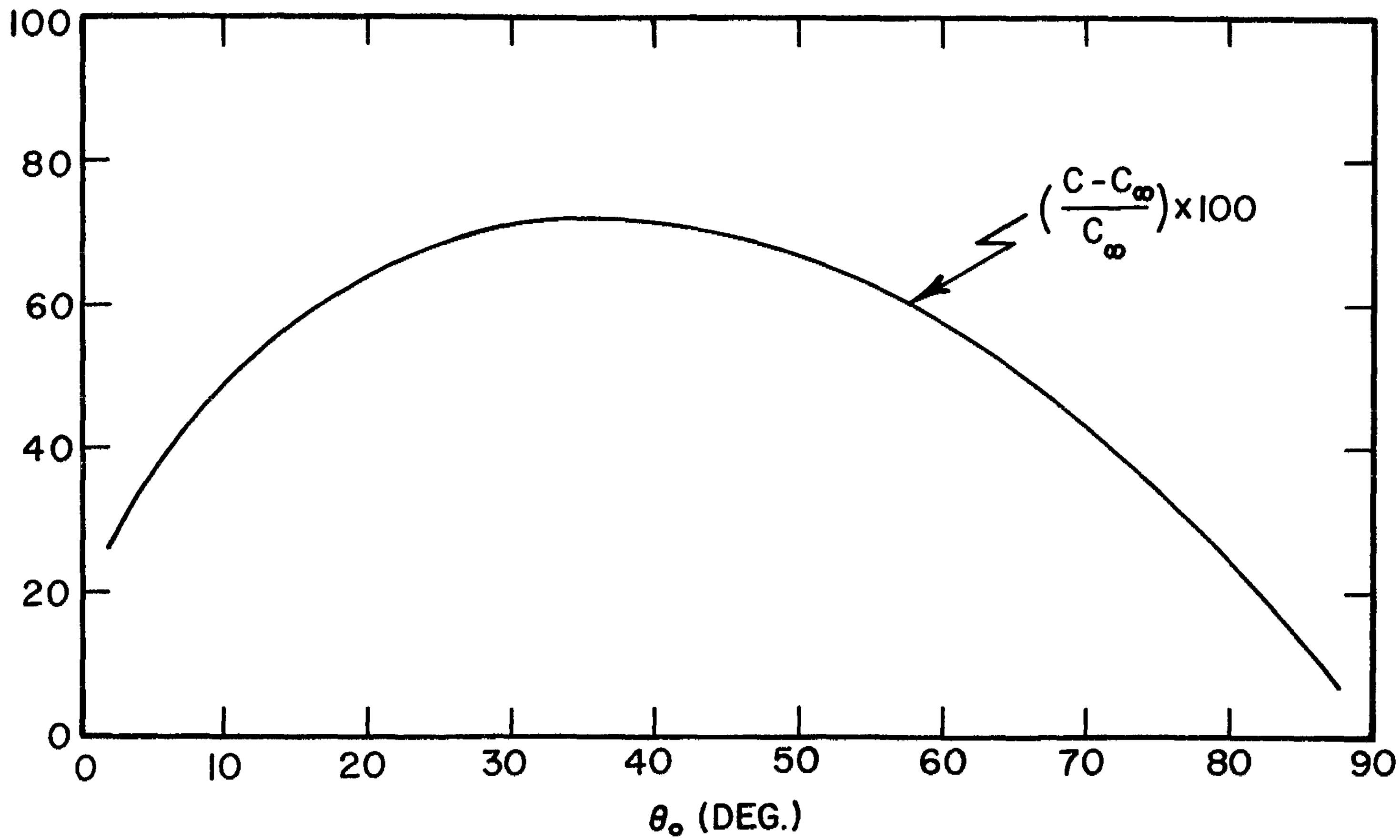

Figure 12. Percentage of fringing capacitance for a cone with a topcap.

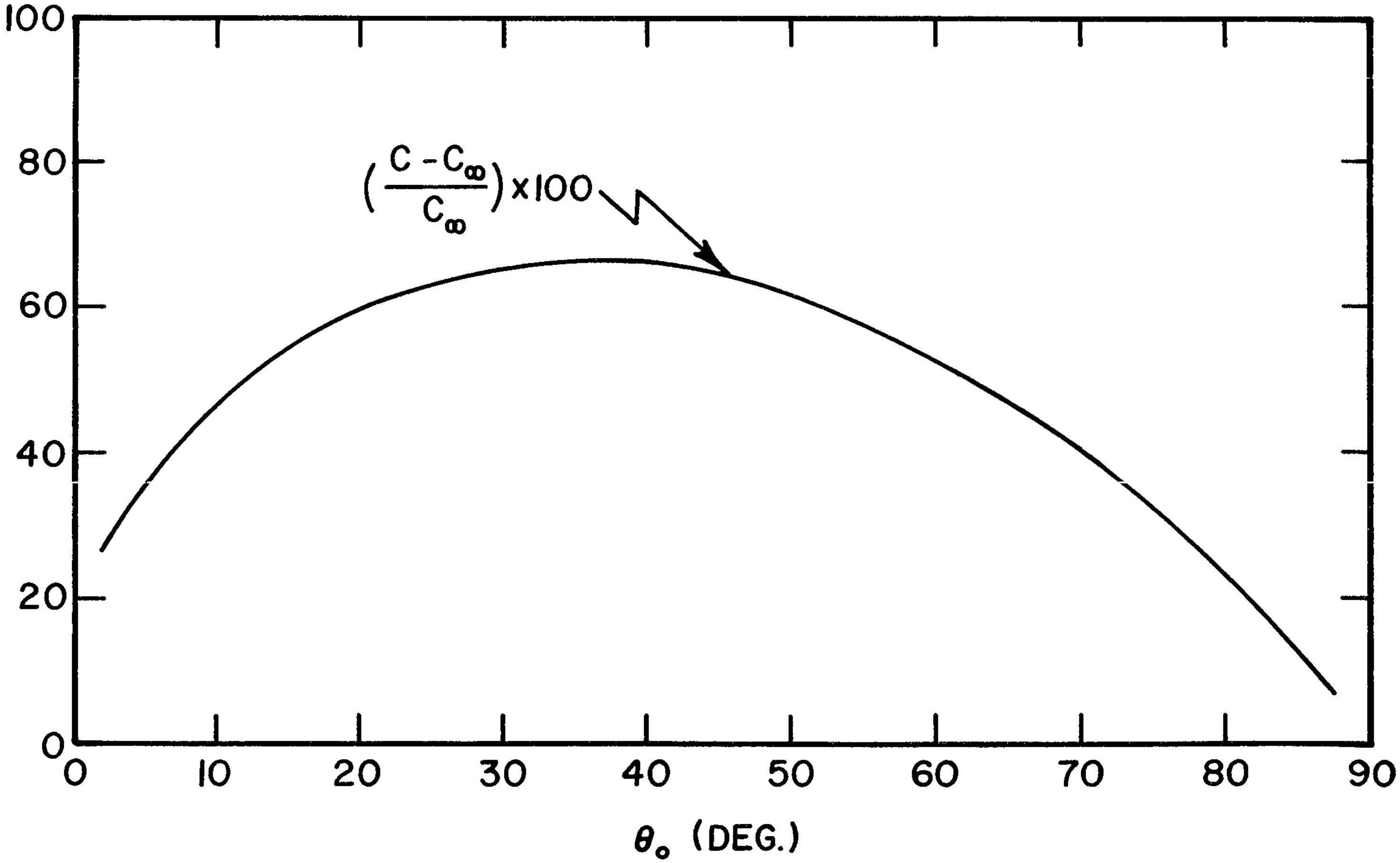

Figure 13. Percentage of fringing capacitance for a cone without a topcap.

Table 2. Computed Effective Height of a Cone over a Conducting Ground Plane

θ_0	With Topcap		Without Topcap	
	h_{eff}/L	$h_{eff}/L \cos\theta_0$	h_{eff}/L	$h_{eff}/L \cos\theta_0$
2.5°	0.5750	0.5755	0.5706	0.5712
5.0°	0.5962	0.5985	0.5893	0.5915
10.0°	0.6195	0.6291	0.6075	0.6169
15.0°	0.6275	0.6496	0.6109	0.6325
20.0°	0.6246	0.6647	0.6038	0.6426
30.0°	0.5916	0.6831	0.5649	0.6523
40.0°	0.5286	0.6900	0.4995	0.6521
50.0°	0.4415	0.6869	0.4141	0.6442
60.0°	0.3364	0.6728	0.3144	0.6288
70.0°	0.2206	0.6450	0.2068	0.6048
80.0°	0.1036	0.5966	0.0987	0.5682
85.0°	0.0488	0.5599	0.0472	0.5421
87.5°	0.0234	0.5365	0.0230	0.5270

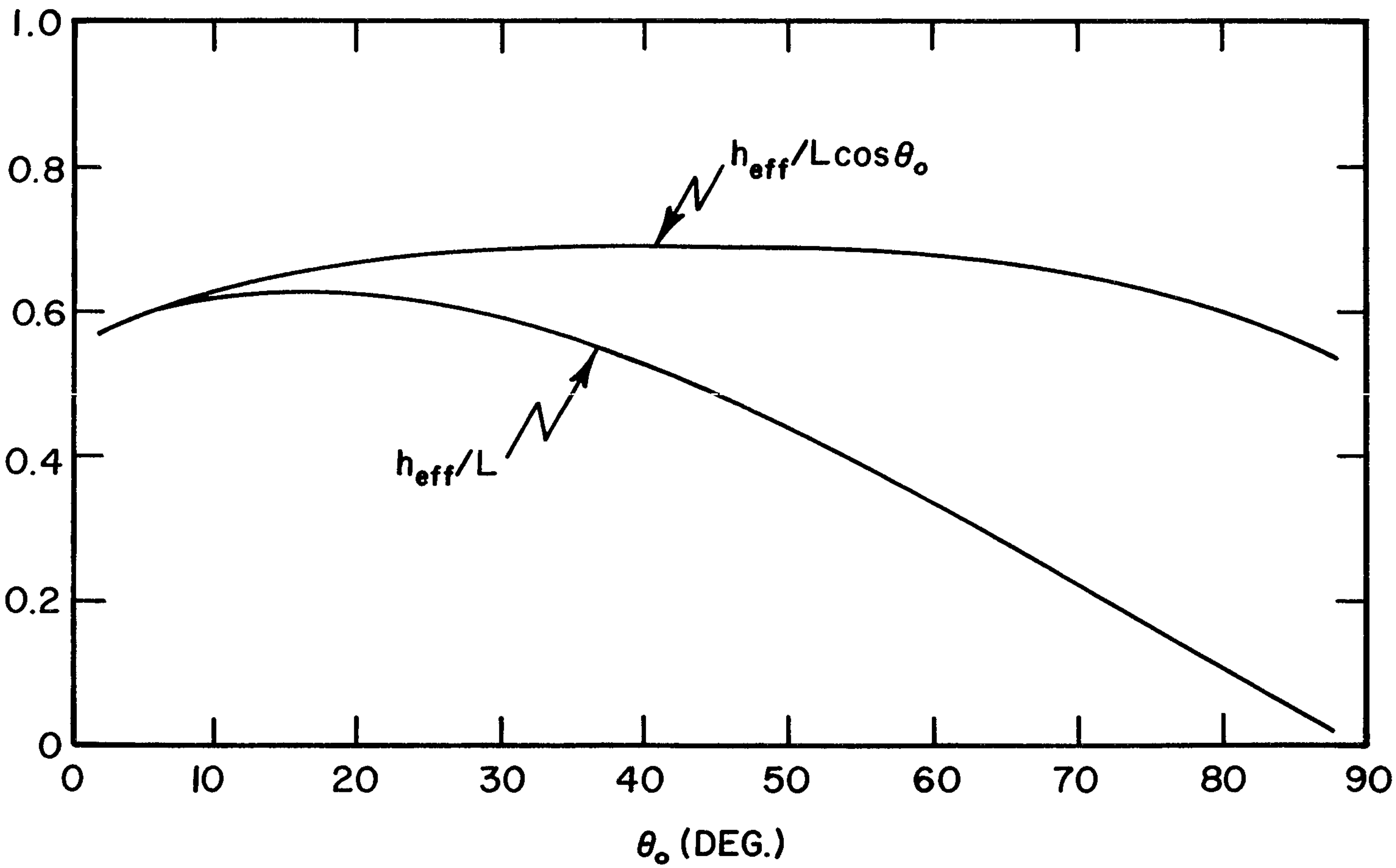

Figure 14. Effective height of a cone with a topcap.

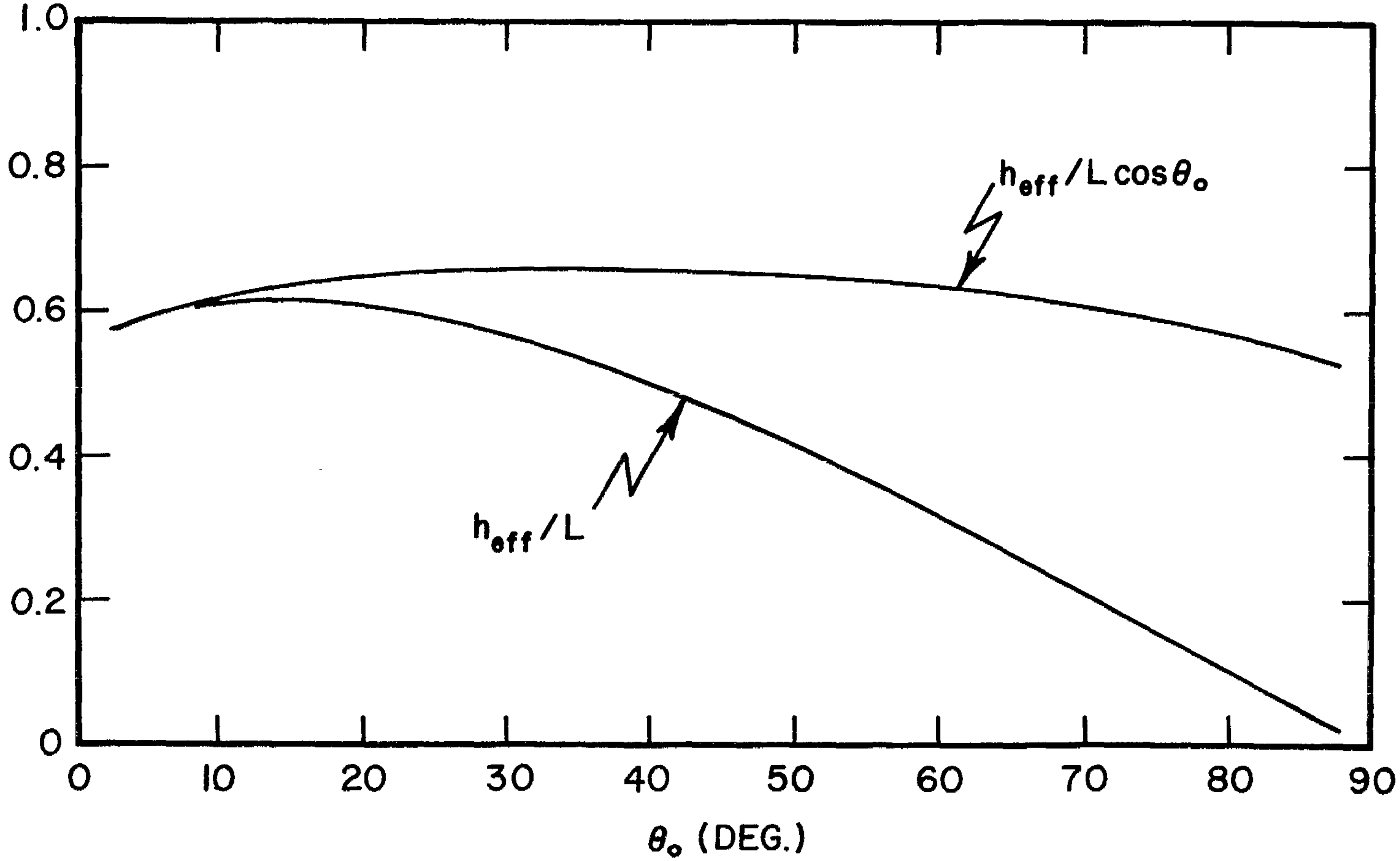

Figure 15. Effective height of a cone without a topcap.

This can easily be seen in Figures 14 and 15 which plot the effective heights as a function of cone angle. Note that the addition of a topcap increases the effective height by about 7%, maximum. This is also in fair agreement with the rough estimate of [3].

SECTION IV

CONCLUSIONS

An integral equation has been derived and numerically solved for the static charge on a conical antenna over a ground plane, both with and without a topcap. Capacitance and effective height data show that there is almost negligible increase in the capacitance when a topcap is added to the conical structure and that there is but a slight increase in the effective height.

Future studies should concentrate on refinements of the model, which should include a more accurate modeling of the wire cage structure and include the circumferential wires. The effect of tapering the bicone angle should also be analyzed and a more accurate model of the feed region should be employed. This improved model should yield more accurate data for the design of biconical structures for use as simulators.

REFERENCES

1. R.F. Harrington, Field Computation by Moment Methods, Macmillan, New York, 1968.

2. D.S. Jones, The Theory of Electromagnetism, Pergamon, London, 1964.

3. W.S. Kehrer and C.E. Baum, "Electromagnetic Design Parameters for ATHAMAS II," ATHAMAS Memos, Memo No. 4, Air Force Weapons Laboratory, Albuquerque, New Mexico, May, 1975.